Journal of Quantitative Spectroscopy & Radiative Transfer 110 (2009) 986–1004

Contents lists available at ScienceDirect

Journal of Quantitative Spectroscopy & Radiative Transfer

journal homepage: www.elsevier.com/locate/jqsrt

The Polar Environment Atmospheric Research Laboratory UV–visible Ground-Based Spectrometer: First measurements of O_3, NO_2, BrO, and OClO columns

Annemarie Fraser [a,*], Cristen Adams [a], James R. Drummond [b,a], Florence Goutail [c], Gloria Manney [d,e], Kimberly Strong [a]

[a] Department of Physics, University of Toronto, Toronto, Ontario, Canada
[b] Department of Physics and Atmospheric Science, Dalhousie University, Halifax, Nova Scotia, Canada
[c] Service d'Aéronomie du Centre Nationale de la Recherche Scientifique, Verrières le Buisson, France
[d] Jet Propulsion Laboratory, California Institute of Technology, Pasadena, California, USA
[e] New Mexico Institute of Mining and Technology, Socorro, New Mexico, USA

ARTICLE INFO

Article history:
Received 5 September 2008
Received in revised form
25 February 2009
Accepted 26 February 2009

Keywords:
Remote sensing
UV–visible spectroscopy
DOAS
Arctic
Stratosphere
Ozone

ABSTRACT

The PEARL-GBS (Polar Environment Atmospheric Research Laboratory-Ground-Based Spectrometer) was permanently installed at Eureka, Nunavut (80.05°N, 86.42°W) in August 2006 as part of the establishment of PEARL by CANDAC (Canadian Network for the Detection of Atmospheric Change). The instrument is a ground-based, UV–visible, triple-grating spectrometer and is very similar to the UT-GBS (University of Toronto-GBS), which has an 11-year heritage of measurements, including 10 High Arctic field campaigns. From spectra of zenith-scattered sunlight, vertical column densities (VCDs) of ozone and NO_2, and differential slant column densities (DSCDs) of BrO and OCIO can be retrieved. The DSCDs and VCDs of ozone and NO_2 have been compared to the UT-GBS and a SAOZ (Système d'Analyse par Observations Zénitales) following the protocols established by the UV–visible Working Group of the Network for the Detection of Atmospheric Composition Change (NDACC). The PEARL-GBS and UT-GBS comparisons meet all standards, while the comparisons with SAOZ partially meet the standards. The VCDs from the three instruments agree, on average, to within 4% for ozone and 8% for NO_2. The BrO DSCDs from the PEARL-GBS and UT-GBS agree to within 14%. These are within the combined error bars of the instruments. In 2009, the PEARL-GBS and UT-GBS became affiliated with the NDACC measurement programme.

© 2009 Elsevier Ltd. All rights reserved.

1. Introduction

The Polar Environment Atmospheric Research Laboratory (PEARL) is located 15 km from the Eureka Weather Station in Nunavut, Canada (80.05°N, 86.42°W). The facility was established as the Arctic Stratospheric Ozone Observatory (AStrO) by Environment Canada in 1993. In 2005, it was taken over by the Canadian Network for the Detection of Atmospheric Change (CANDAC) and expanded with the addition of two facilities and a suite of new instrumentation. Eureka is part of the primary Arctic station of the Network for the Detection of Atmospheric Composition Change (NDACC).

* Corresponding author at: School of GeoSciences, University of Edinburgh, Edinburgh, UK.
E-mail address: ac.fraser@ed.ac.uk (A. Fraser).

0022-4073/$ - see front matter © 2009 Elsevier Ltd. All rights reserved.
doi:10.1016/j.jqsrt.2009.02.034

As part of the refurbishment of PEARL, a UV–visible diffraction grating spectrometer, the PEARL-GBS (PEARL-Ground-Based Spectrometer) was permanently installed at PEARL in August 2006 and has since recorded data continuously, except during polar night. Prior to this installation, UV–visible zenith-sky measurements at Eureka were only made on a campaign basis. Vertical column densities (VCDs) of ozone and NO_2 and differential slant column densities (DSCDs) of BrO and OClO can be retrieved from the spectra. The instrument was developed following the UT-GBS (University of Toronto-GBS), which has an 11-year heritage of measurements, including four mid-latitude [1–3] and 10 High Arctic field campaigns [4–6].

The Antarctic ozone hole was discovered by examining total ozone data recorded at Halley Bay, Antarctica from 1957 onwards [7]. Since the initial discovery, the processes controlling seasonal ozone loss have become well known [e.g. 8]. Seasonal ozone loss in the Arctic also occurs, though it is not as severe because of warmer, more dynamically active conditions there, which are in turn related to larger variations in the underlying topography. Measurements by the PEARL-GBS and UT-GBS allow for the characterization of the chemical composition of the stratosphere over Eureka during both chemically perturbed and unperturbed conditions, as well as the investigation of seasonal and interannual variability of the ozone budget. Measurements of BrO are particularly important: bromine chemistry is not as well understood as that of the other halogens. A lack of measurements of BrO, specifically at high latitudes, means that most of the current understanding of bromine chemistry comes from model calculations [e.g. 9].

This paper describes the new instrument and the data processing technique, presents the data from the first 14 months of operation, discusses comparisons between the data retrieved from this instrument and other instruments operating at PEARL, and finally discusses future measurement plans.

2. Instrument

The PEARL-GBS is a crossed Czerny-Turner diffraction grating imaging spectrometer (TRIAX 180, Jobin Yvon Inc.). A schematic is shown in Fig. 1. The instrument primarily operates in zenith-sky mode, and sunlight is gathered by a fused silica lens of 40-mm diameter (f-number 2.5) and a 2° field-of-view. Light is then focused onto a 1-m-long liquid light guide (LLG) with an inner core diameter of 3 mm (f-number 0.85). The LLG depolarizes the light, while bringing it into the f-number matcher, a series of lenses that first collimates the light, and then focuses it onto the slit of the spectrometer (f-number 3.9). A six-position filter wheel is installed between the f-number matcher and the spectrometer. Four filters were installed during the measuring period: blue green (band pass 350–600 nm), long wave (band pass >575 nm), black (band pass 250–400 nm), and neutral density (0.1% transmission).

The spectrometer consists of two aspherical mirrors and three holographic or ruled plane gratings. The light passes through a fixed slit (0.05 mm) and mechanized shutter, and is then collimated by a mirror onto one of the three gratings. The second mirror focuses the dispersed light onto the charged coupled device (CCD) detector. The focal length of the instrument is 0.190 m, with a focal plane of 30 mm $\times$ 12 mm. The typical sampling of spectral lines, resolution, wavelength ranges, and typical wavelength limits of the gratings are shown in Table 1. These line shapes are regularly measured using a set of three calibration lamps, and has been found to be constant with time, although it does vary across the CCD, increasing in width towards the edges.

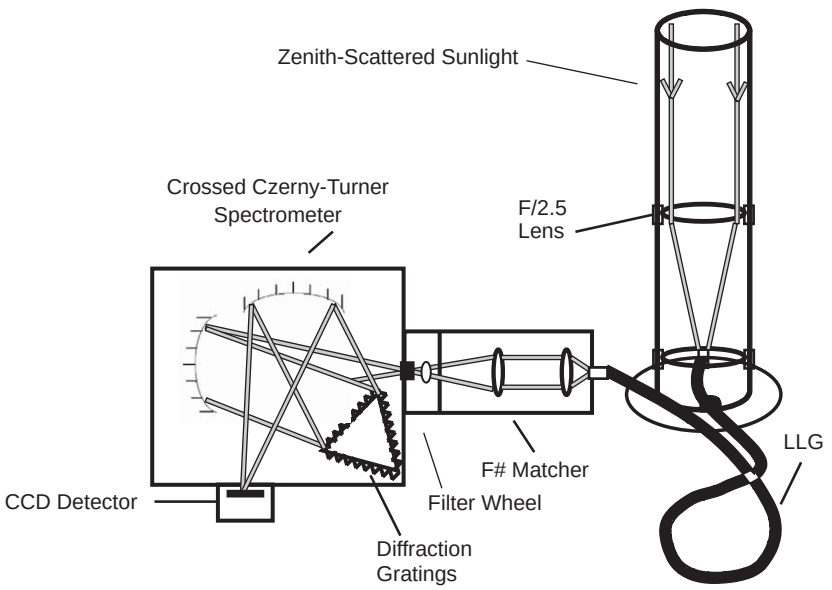

Fig. 1. Schematic of the PEARL-GBS.

Table 1
Sampling of spectral lines, resolution, wavelength ranges, and typical wavelength limits for the three gratings of the PEARL-GBS.

Grating (gr/mm)	Sampling (pixels/FWHM)	Resolution (nm)	Wavelength range (nm)	Usual wavelength limits (nm)
300	5–14	1.0–3.0	440	300–740
600	4.5–16	0.5–2.5	210	340–550
1200	7–12	0.2–0.8	100	330–430

Table 2
Details of the WinDOAS analysis for the UT-GBS and PEARL-GBS.

Species	Grating (gr/mm)	CPD	CWL (nm)	# of SW	CF	Offset
Ozone	600	3	400–550	5	0, 1, 2, 3	None
NO_2	600	3	400–550	5	0, 1, 2, 3	None
NO_2	1200	3	380–420	5	0, 1, 2, 3	Quadratic
BrO	600	2	350–400	3	0, 1, 2, 3	Quadratic
BrO	1200	2	340–400	3	0, 1, 2, 3	Quadratic
OClO	1200	3	340–390	5	0, 1, 2, 3	Quadratic

The same polynomial degree is used in the calibration for both the wavelength shift and the slit function parameters, and is given in the column CDP (calibration polynomial degree). CWL (calibration window limit) is the range used for the wavelength calibration and is not the wavelength region used in the spectral fitting. # of SW is the number of subwindows used in the wavelength calibration. CF (continuous functions) is the degree of polynomial fit to the optical depth in the DOAS analysis (0, 1, 2, 3 indicates a polynomial of the form $a + bx + cx^2 + dx^3$).

The CCD detector (Symphony, Jobin Yvon Inc.) is a back-illuminated two-dimensional array, with 2048 × 512 pixels, and a physical size of 27.6 × 6.9 mm. Each pixel is 13.5 μm × 13.5 μm. It has a four-stage Peltier thermo-electric cooling system, and operates at a temperature between 202 and 205 K. The CCD is coated with an enhanced broadband coating, and has a quantum efficiency ranging from 50% at 300 nm to 90% at 400 nm and 80% at 600 nm.

The instrument is controlled by a computer running LabVIEW software. Spectra are created by binning the 512 pixels along the vertical axis of the CCD. Data are recorded continuously, with varying exposure times, optimized based on an initial test measurement, to maximize the amount of signal on the CCD, with a maximum of 300 s to limit smearing over solar zenith angles (SZAs). When the SZA is smaller than 80°, spectra are limited to once every 15 min.

The instrument is located inside a hatch on the roof of PEARL, with a UV-transmitting plexiglas window to view the zenith-sky. In August 2007, this was replaced with a UV-transmitting plexiglas dome. Generally the instrument is operated using the 600 grooves/mm grating, with a wavelength range of 340–550 nm, allowing the retrieval of ozone (450–450 nm), NO_2 (425–450 nm), and elevated BrO (345–360 nm). From March to May 2007, the 1200 grooves/mm grating was used, with a wavelength range of 330–430 nm, focusing on the BrO and OClO (345–390 nm) regions. NO_2 can be retrieved from this grating as well, using wavelengths between 400 and 430 nm.

The UT-GBS is an essentially identical instrument to the PEARL-GBS. It does not have a filter wheel, and the slit, instead of being fixed, is motorized, and can be set to any width. In practice, it is set to 0.05 mm. The CCD has a different coating, with a quantum efficiency ranging from 50% at 350 nm to 70% at 500 nm.

The dark current and bias of both instruments are regularly measured, and have been found to be constant with time.

3. Data analysis

The DOAS (Differential Optical Absorption Spectroscopy) technique [10,11] is used for the analysis of the spectra from both the UT-GBS and PEARL-GBS, with absorption cross-sections of ozone [12], NO_2 [13], H_2O [14], O_4 [15], BrO [16], OClO [17], and the Ring cross-section [18] fitted using a Marquardt–Levenberg non-linear least-squares technique. The Ring effect is the filling in of Fraunhofer lines due to Raman scattering of sunlight. The Ring cross-section is calculated by convolving a high-resolution solar spectrum with rotational Raman spectra of O_2 and N_2.

For the 600 gr/mm grating, ozone is fitted between 450 and 550 nm, NO_2 between 425 and 450 nm, and BrO between 345 and 360 nm. For the 1200 gr/mm grating, NO_2 is fitted between 400 and 430 nm, BrO between 345 and 360 nm, and OClO between 350 and 390 nm. For NO_2 and BrO, the fitting recommendations of Vandale et al. [19] and Aliwell et al. [20] are also followed.

The programme WinDOAS, developed by the IASB-BIRA (Belgian Institute for Space Aeronomy) [21], is used to analyse the spectra. Spectra are corrected for dark current and bias prior to the analysis. WinDOAS applies a fitted offset correction during the analysis. The offset is a polynomial added to the intensity of the wavelength-calibrated spectra to account for stray light in the instrument. Table 2 gives the details of the WinDOAS analysis for the PEARL-GBS and UT-GBS. These settings were chosen to optimize the fits for the different species. The Gaussian slit function is fit in each of the calibration subwindows and is used to smooth the high-resolution cross-sections to the resolution of the instrument. The quality of

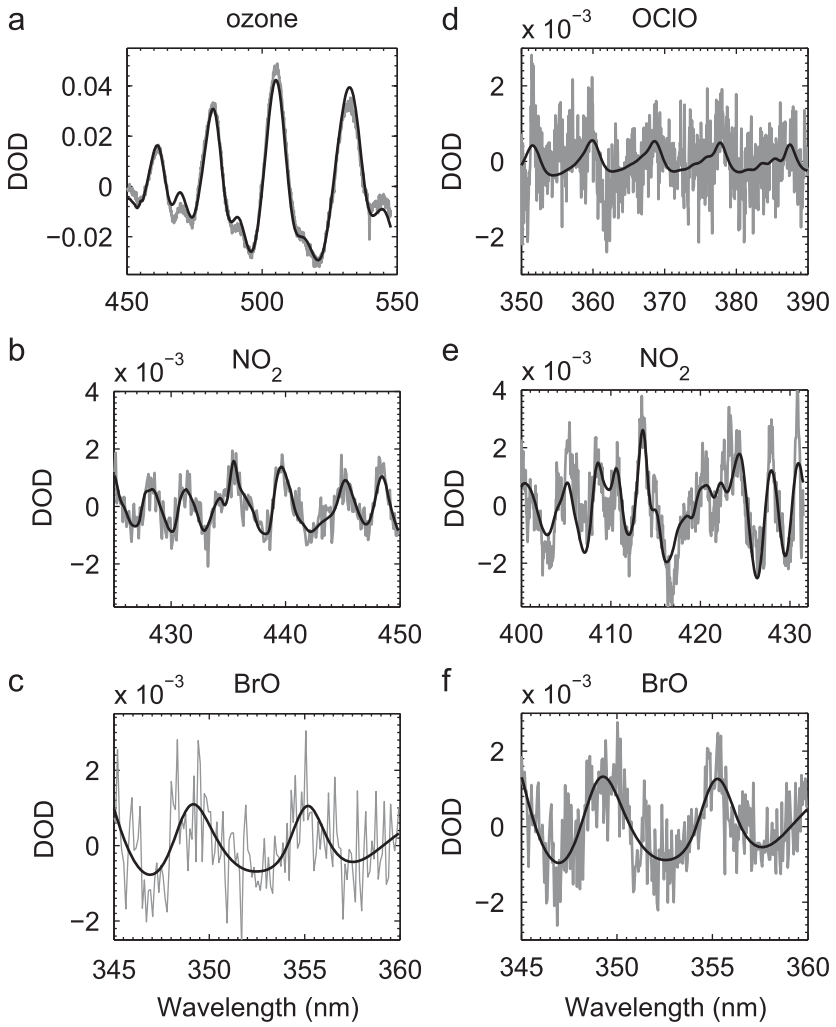

Fig. 2. Differential optical depth (DOD) fits for the PEARL-GBS for (a) ozone, (b) NO_2, and (c) BrO for February 27, 2007 using the 600 gr/mm grating. DOD fits for (d) OClO, (e) NO_2, and (f) BrO for March 5, 2007 using the 1200 gr/mm grating. All fits are for a SZA of approximately 90° in the evening, with a reference spectrum at 88° for February 27 and 86° for March 5. The grey line is the data, while the black line is the fit to the data.

the fits is improved by allowing WinDOAS to fit the slit function. The wavelength calibration is performed on both the reference and twilight spectra. The wavelength calibration algorithm used in WinDOAS performs a non-linear least-squares fit, using the Marquardt–Levenberg algorithm, to the reference spectrum. This is done using Fraunhofer lines from an accurately calibrated high-resolution solar spectrum which is first degraded to the resolution of the instrument. The degree of the polynomial fit to the optical depth in the DOAS analysis is given by the continuous function.

Fig. 2 shows examples of typical differential optical depth fits for ozone, NO_2, BrO, and OClO. Daily reference spectra are used: for ozone and NO_2, the spectrum recorded at the smallest SZA is used, while for BrO and OClO, the spectrum at 80° (where available) is used. Fig. 3 shows typical variations in DSCD with SZA for the four species. The observed scatter of the BrO DSCDs compared to those of OClO may indicate a significant and variable tropospheric BrO contribution.

3.1. Vertical column densities

The conversion of ozone and NO_2 DSCDs into VCDs is based on the following relationship:

$$DSCD(SZA) = VCD(SZA) \times AMF(SZA) - RCD. \quad (1)$$

RCD is the reference slant column density, the amount of absorber in the reference spectrum, and AMF is the air mass factor, a measure of the path length through the atmosphere. The AMF is calculated from a one-dimensional vector radiative transfer model. Included in the model are vertical profiles of ozone, NO_2, BrO, aerosols, temperature, and density [22]. Density, temperature, and ozone profiles are taken from weekly (daily during late February to mid-March)

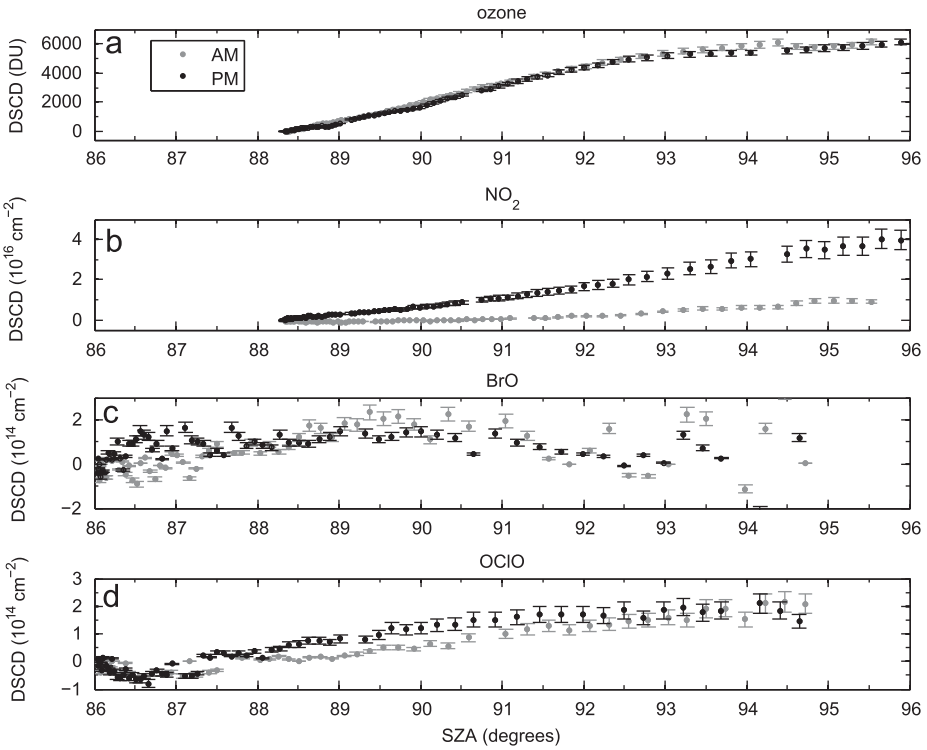

Fig. 3. DSCD versus SZA for (a) ozone, (b) NO_2, (c) BrO, and (d) OClO. Ozone and NO_2 plots are for February 27, 2007. BrO and OClO are for March 5, 2007.

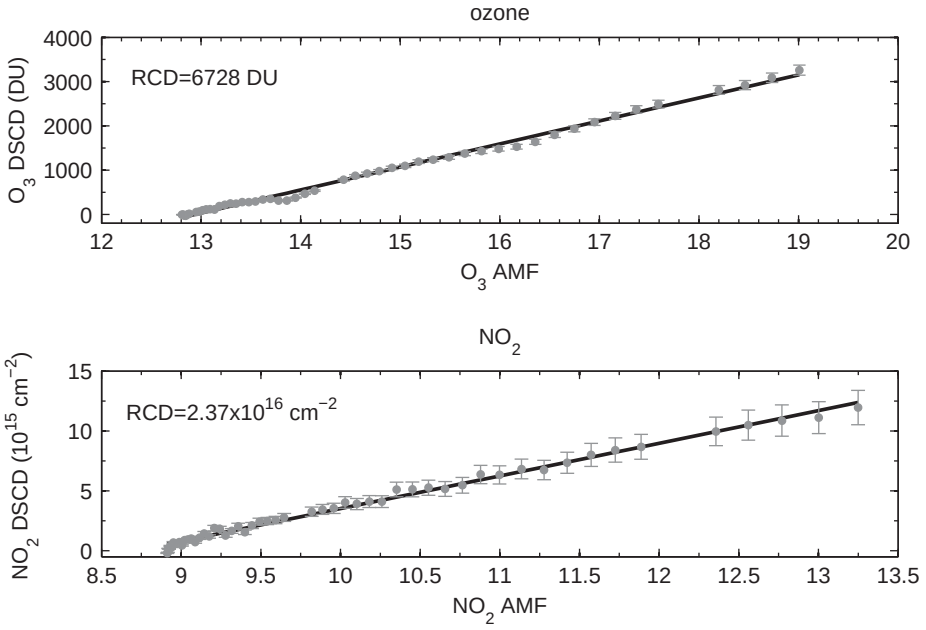

Fig. 4. Langley plots of DSCD versus AMF for (a) ozone and (b) NO_2 for the afternoon of February 27, 2007. In all plots, the points represent the data, while the line is the fit to the data. The RCD is also given for both species.

ozonesondes flown from Eureka. The aerosol profile is taken from a SAGE II (Stratospheric Aerosol and Gas Experiment) profile recorded in 1997. The NO_2 and BrO profiles are taken from the University of California at Irvine (UCI) photochemical box model for 75°N and for the month of the measurement [23,24].

Table 3
Measurement errors for the PEARL-GBS.

Source of error	O_3 (%)	NO_2 (%)	BrO (%)	OClO (%)
Random noise	1	2	5	7.5
Instrument error	1	1	1	1
Pseudo-random errors	1–2[a]	4–6[a]	10	10
Absolute cross sections	2.6[b]	5[c]	8[d]	7[e]
Temperature dependence of cross sections	–	<8[f]	2[g]	7[e]
Filling in of absorption by Raman scattering	1[h]	5[h]	5[h]	5[h]
Total RMS error DSCD	3.5	12.0	14.8	16.7
AMF error	2[a]	5[a]	–	–
Uncertainty in RCD	1	10	–	–
Total RMS error VCD	4.1	16.4	–	–

[a] Bassford et al. [2].
[b] Burrows et al. [12].
[c] Vandaele et al. [13].
[d] Wilmouth et al. [16].
[e] Wahner et al. [17].
[f] Pfeilsticker et al. [28].
[g] Harder et al. [29].
[h] Fish and Jones [28], Pfeilsticker et al. [30].

For ozone and NO_2, a Langley plot of DSCD vs. AMF is made for each twilight period, and the RCD is found by performing a straight line fit to the data. Fig. 4 shows a sample Langley plot for the two species. The ordinate of the line is the negative of the RCD, as seen in Eq. (1). An average RCD is found for each day by averaging the morning and afternoon values. Each DSCD is then converted into a VCD using Eq. (1), and the VCD for a twilight period is taken as the average of all the VCDs. Generally only DSCDs from SZAs between 86° and 91° are used [25]. Since NO_2 has a diurnal variation, the VCD is an average of the VCDs over the twilight period.

For BrO, the DSCD at a SZA of 90° is interpolated from each set of twilight measurements. BrO has a strong diurnal cycle: because of this, calculations of the VCD and RCD are more difficult than for ozone and NO_2. This is further complicated by the small range of SZAs available at Eureka. As a result, BrO VCDs are not calculated here. The approximate AMF from the radiative transfer model ranges between 10 and 13 at 90°.

OClO is not long-lived in the sunlit atmosphere, and so the AMF is difficult to determine. As a result, only DSCDs can be found for OClO. Models show an approximate value of 10 at 90° in the Arctic [26,27]. As for BrO, the DSCD at 90° is interpolated from each set of twilight measurements.

3.2. Sources of error

Measurement errors are calculated as a percentage of the column amount from the root-mean-square (RMS) of individual sources of random and systematic error, after Bassford et al. [2] and references therein. Table 3 gives the estimated values of the individual error for the PEARL-GBS. When the value represents a best estimate taken from the literature, a reference is given in the table. All other values are calculated from the measurements.

Errors in the DSCDs stem from random noise on the spectra, instrument error, pseudo-random errors, errors in the absorption cross-sections, the temperature dependence of the cross-sections, and the effects of multiple Raman scattering. Instrument errors arise from uncertainties in the bias and dark current of the instrument, as well as the effects of stray light. These instrument errors add an offset to the spectra. Pseudo-random errors result in unaccounted-for structure in the spectra, and are a result of errors in the characterization of the slit function, interpolation, and the wavelength calibration of the spectra and the effects of polarization. If not properly corrected for, these errors add an additional signal containing spectral structure to the spectra that is not included in the DOAS analysis. NO_2, BrO, and OClO cross-sections are all sensitive to the temperature of the atmosphere. A single cross-section for each species was chosen at a reasonable temperature for the stratosphere, which introduces uncertainties into the fitted DSCDs. No correction has been made for the filling-in of absorption features by multiple Raman scattering. Pfeilstickler et al. [28] show that this effect can result in an underestimation of NO_2 columns by 5% and ozone columns by 1%. The NO_2 value is taken here for BrO and OClO.

VCD errors combine the DSCD errors, uncertainties in the AMF, and uncertainty in determining the RCD. Uncertainties in the AMF were derived by Bassford et al. [1] for ozone and NO_2. The uncertainty in the RCD is derived by varying the RCD from the smallest to largest value from the campaign and observing the variation caused in the VCD, calculated as described in Section 3.1.

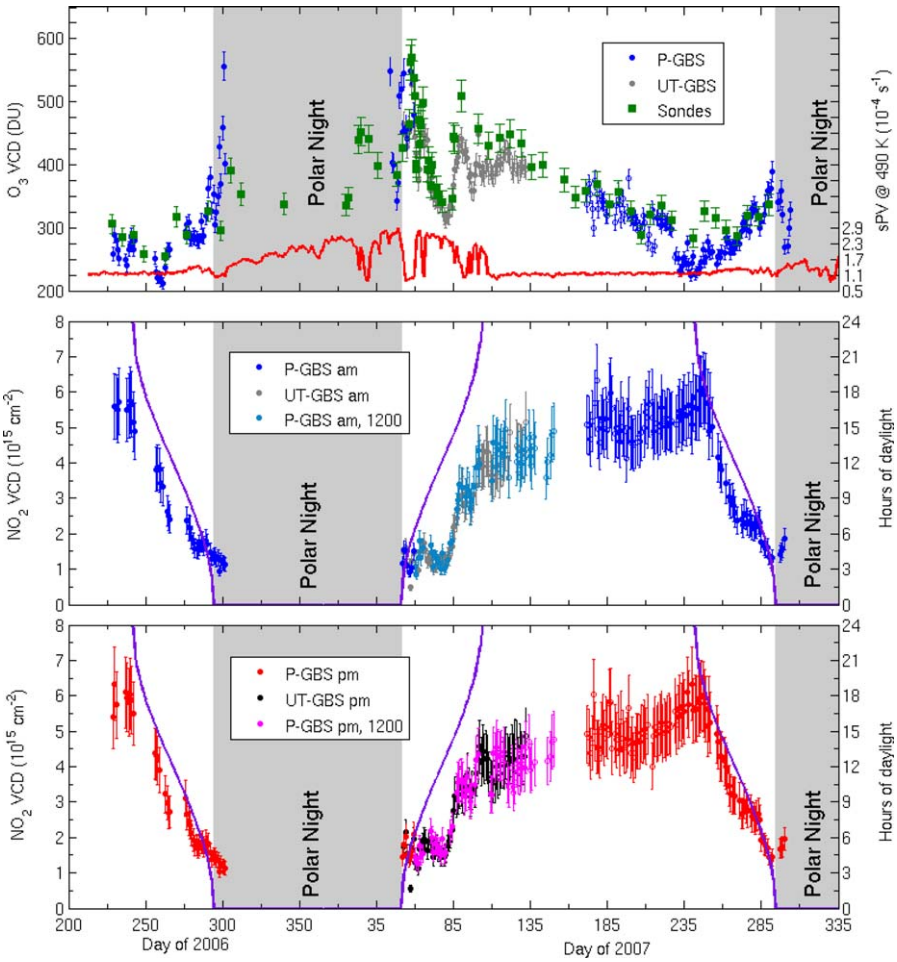

Fig. 5. (a) Daily average ozone VCDs from the PEARL-GBS, UT-GBS, and ozonesondes from August 2006 to October 2007. The red line is the sPV on the 490 K potential temperature level. (b) NO_2 AM VCDs from the PEARL-GBS (P-GBS in the legend) and UT-GBS from August 2006 to October 2007. The purple line is the total hours of daylight. (c) as (b) but for PM VCDs. The open symbols on all three panels indicate the days where VCDs are calculated using all available SZAs, because the Sun is not in the 86–91° range. (For interpretation of the references to colour in this figure legend, the reader is referred to the web version of this article.)

4. Results from the first year of measurements

The PEARL-GBS was permanently installed at Eureka in August 2006. The instrument has made continuous measurements since then, with the exception of during polar night (November–February), a few days in September 2006, and a period in June 2007 when instrument problems prevented measurements. During the majority of the Canadian Arctic ACE (Atmospheric Chemistry Experiment) Validation Campaign in spring 2007, it was operated with the 1200 gr/mm grating, and ozone measurements were not possible. Except for these periods, there is a continuous ozone and NO_2 VCD record from the installation to the beginning of polar night in fall 2007. With the addition of ozone data from the UT-GBS, which participated in the ACE campaign, the ozone record is extended through the 2007 campaign. The UT-GBS is also deployed inside a hatch at PEARL under a plexiglas window.

Fig. 5(a) shows the daily average of morning and evening ozone VCDs from the PEARL-GBS and UT-GBS from August 2006 to October 2007. Also shown are the weekly (daily during late February and early March) ozonesondes launched from the Weather Station. The ozonesonde profiles have been integrated to give the column, with a correction added to account for the ozone above the balloon burst height [31]. Errors on the ozonesonde total columns are 5% [32]. Because the Sun travels through a limited range of SZAs in the course of a day at Eureka, in the summer when the Sun is continuously above the horizon, the preferred SZA range for calculating the VCD is not always available. During this time, all available SZAs are used. This period is denoted by open symbols in Fig. 5, and runs between days 105 (April 15) and 230 (August 18). Fig. 6 shows the maximum and minimum SZAs at Eureka throughout the year.

The sPV (scaled potential vorticity) on the 490 K potential temperature level ($\sim$18 km) at the latitude and longitude of Eureka is also shown in Fig. 5. sPV is calculated from GEOS-5 (Goddard Earth Observing System) reanalysis data for local

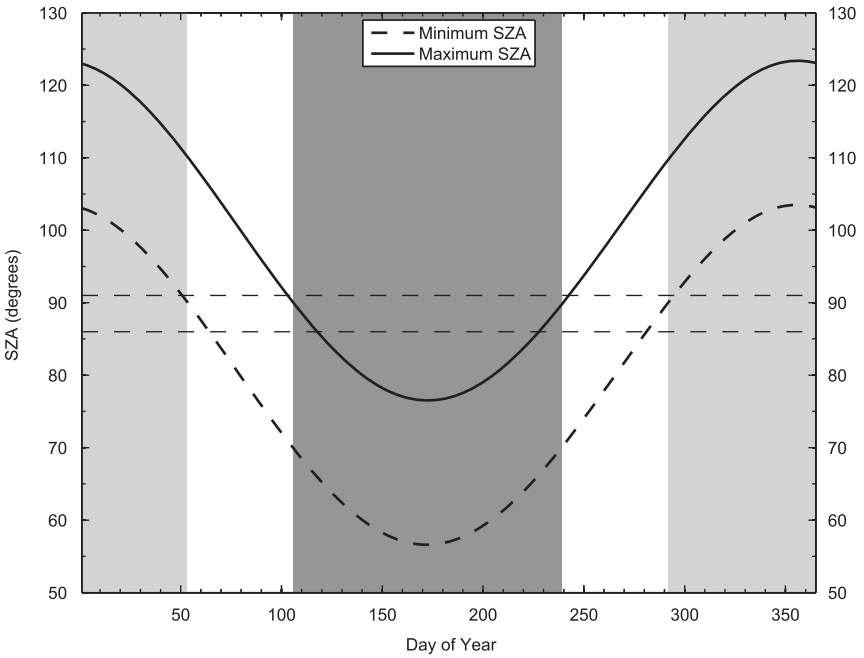

Fig. 6. Maximum and minimum SZAs at Eureka throughout the year, calculated for 2007. The light gray shaded region indicates polar night, when the Sun does not rise above the horizon, while the dark gray shaded area indicates the time of year when the Sun is continuously above the horizon. The horizontal dotted lines indicate 86° and 91°, the preferred range of SZAs used in the calculation of VCDs.

noon at the latitude and longitude of Eureka [33,34]. A description of how sPV is calculated is given in Manney et al. [35]. To first order, sPV values below $1.2 \times 10^{-4}\,s^{-1}$ indicate that Eureka is outside the vortex, while those above $1.6 \times 10^{-4}\,s^{-1}$ indicate that Eureka is inside the vortex. In between these values, Eureka is on the edge of the vortex [35].

At the end of 2006, the polar vortex begins to form over Eureka in mid-October and gains strength throughout the polar night. The winter of 2006/2007 had a strong polar vortex located over the pole, with Eureka spending significant time inside the vortex. Maps of total ozone columns from the Science and Technology branch of Environment Canada (available at http://exp-studies.tor.ec.gc.ca/e/ozone/ozone.htm, created using observations from ground-based Brewer spectrophotometers and satellite data from the Total Ozone Mapping Spectrometer) show that a region of high ozone was located to the west of Eureka, outside of the vortex, during February and March 2007, which was transported back and forth over Eureka as the vortex moved overhead. During March, the polar vortex moved over Eureka and remained there until the final warming began at the end of March. By the beginning of April, the vortex has completely broken apart. At the end of 2007, the polar vortex begins to form in mid-October, gaining strength until mid-November, when the vortex moves away from Eureka.

During springtime, the ozone columns are largely determined by the position of the vortex with respect to Eureka, as indicated by the sPV values. This period will be more closely examined in the following section. Once the vortex breaks apart, the VCDs are constant for roughly a month, and then decrease throughout the summer until the end of August. Ozone decreases through the summer due to the weakened descent of ozone in the polar regions at this time of year, as well as an increase in tropopause height. In the fall, as both the transport from midlatitudes and descent strengthen, ozone concentrations begin to increase [e.g. 37]. As seen in Fig. 5(a), in 2006, the period of increasing ozone begins in mid-September (day 255), while in 2007 it begins in late August (day 235). In both years, ozone VCDs increase steadily through the fall until the beginning of polar night. In the late fall the polar vortex reforms, and concentrations are again determined by the position of the vortex. In 2006, the VCDs continue to increase at the start of polar night as the forming polar vortex moves further away from Eureka. In 2007, the VCDs begin to decrease after the Sun sets, while the sPV increases.

Fig. 5(b) and (c) shows the NO_2 AM and PM VCDs, respectively, from the PEARL-GBS and UT-GBS from August 2006 to October 2007. As in Fig. 5(a), open symbols are used when the Sun does not set below 86°. Also shown in these figures is the number of hours of daylight (defined as when the SZA is less than 90°). NO_2 is formed throughout the day, as N_2O_5 is photolysed. The amount of daylight is the dominant factor in determining the NO_2 columns. Other factors include the temperature dependence of the photolysis of N_2O_5 and the amount of NO_3 available for the production of N_2O_5. As the amount of available sunlight decreases in the fall and increases in the spring, the columns of NO_2 quickly decrease and increase, respectively. In the spring, the recovery of NO_2 is complicated by the position of the vortex, and will be further discussed in the following section. Once the vortex breaks apart, the NO_2 VCDs steadily increase, leveling off near the end of June to remain relatively constant over the summer. At the end of August, the Sun sets for the first time since April, and the VCDs rapidly decrease. In both years, the NO_2 VCDs steadily decrease until the beginning of polar night. In 2006,

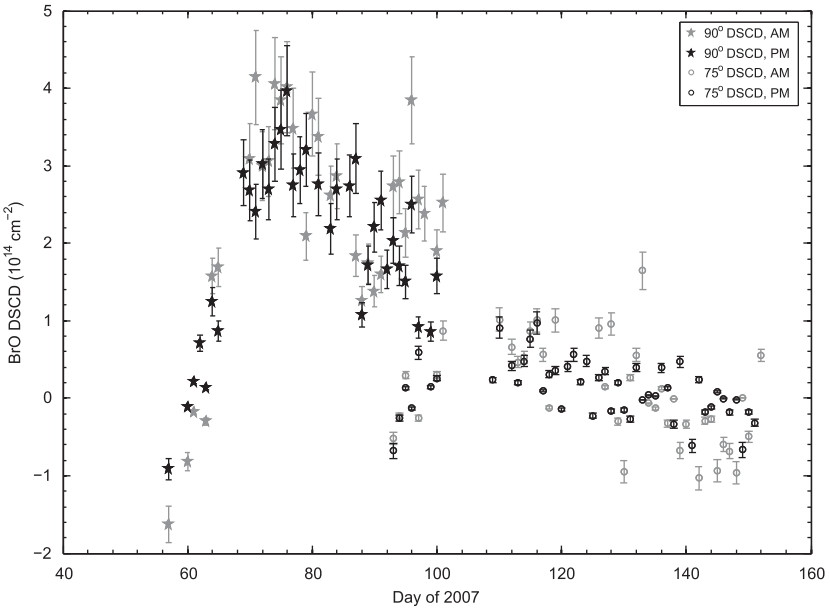

Fig. 7. BrO DSCDs from February to June 2007. DSCDs at both 90° and 75° are shown.

concentrations then continue to decrease, while in 2007, concentrations start to increase. This behaviour corresponds to the behaviour of the ozone VCDs, and is related to the position of the newly forming polar vortex. Outside of polar springtime, ozone and NO_2 VCDs are negatively correlated, with a correlation coefficient, r, of −0.6. This negative relationship is expected and is mainly due to the transport of mid-latitude air into the polar regions.

Fig. 7 shows the BrO DSCDs calculated at 90° and 75° using a daily reference spectrum from the highest possible SZA. Negative values indicate that the reference spectrum is taken at a SZA close to 90° or 75°, so the DSCD is very small. The 600 gr/mm grating is used until February 28 (day 59), after which the 1200 gr/mm grating is used. After June 1 (day 152), the instrument resumed using the 600 gr/mm grating, to allow for ozone measurements through the summer. After day 105, the Sun no longer reaches 90°, and so a DSCD at 90° can no longer be calculated. BrO DSCDs had decreased significantly from the maximum observed in March, and were too small to be measured accurately with the 600 gr/mm grating during the summer. Although BrO concentrations begin to increase in the fall, the concentration remains too small for accurate DSCD measurements. The 75° DSCDs show the continued decrease and leveling off of the BrO columns expected through the summer.

The seasonal variation in BrO, generally increasing until mid-March and then decreasing to the end of spring, is similar to the variation in BrO DSCDs seen at the Arctic sites of Ny-Ålesund (79°N) and Andøya (69°N), Norway and Kiruna, Sweden (68°N) by Sinnhuber et al. [38] for the springs of 1998, 1999, and 2000. Tørnkvist et al. [9] also observed the decrease of springtime BrO. The DSCDs shown here are found using a reference spectrum from the highest possible SZA, while the studies cited use a reference spectrum at a SZA of 80°. Using an 80° reference spectrum, the DSCDs vary between −2 and 4×10^{14} molecules/cm^2, similar to the 0.5–4×10^{14} molecules/cm^2 observed by Tørnkvist et al. [9] and larger than the 0.1–2×10^{14} molecules/cm^2 observed in Ny-Ålesund by Sinnhuber et al. [38]. The Tørnkvist et al. [9] observations are generally inside the vortex, while Sinnhuber et al. [38] do not provide the meteorology of the observing conditions. Tørnkvist et al. [9] observed smaller BrO amounts outside the polar vortex, in agreement with the behaviour seen in Eureka.

The BrO DSCDs vary positively with ozone and negatively with NO_2, with correlation coefficients of 0.4 and −0.4, respectively. Tørnkvist et al. [9] observed a negative correlation between NO_2 and BrO for measurements taken at Ny-Ålesund during two springtime campaigns and Andøya over the course of one year of measurements. Richter et al. [39] also observed a negative correlation in yearly measurements taken at Bremen, Germany (52°N) between 1994 and 1996. Model studies support the expectation of a negative correlation between BrO and NO_2. When concentrations of NO_2 increase, $BrONO_2$ is quickly formed, and BrO concentrations decrease [30,40].

4.1. The 2007 Canadian Arctic ACE Validation Campaign

ACE is a Canadian satellite, launched in August 2003, to investigate the chemical and dynamical processes that are involved in the distribution of ozone in the atmosphere, with a focus on the Canadian Arctic [41]. Six validation campaigns have been held during polar sunrise at PEARL from 2004 to 2009, involving a suite of six to nine ground-based instruments

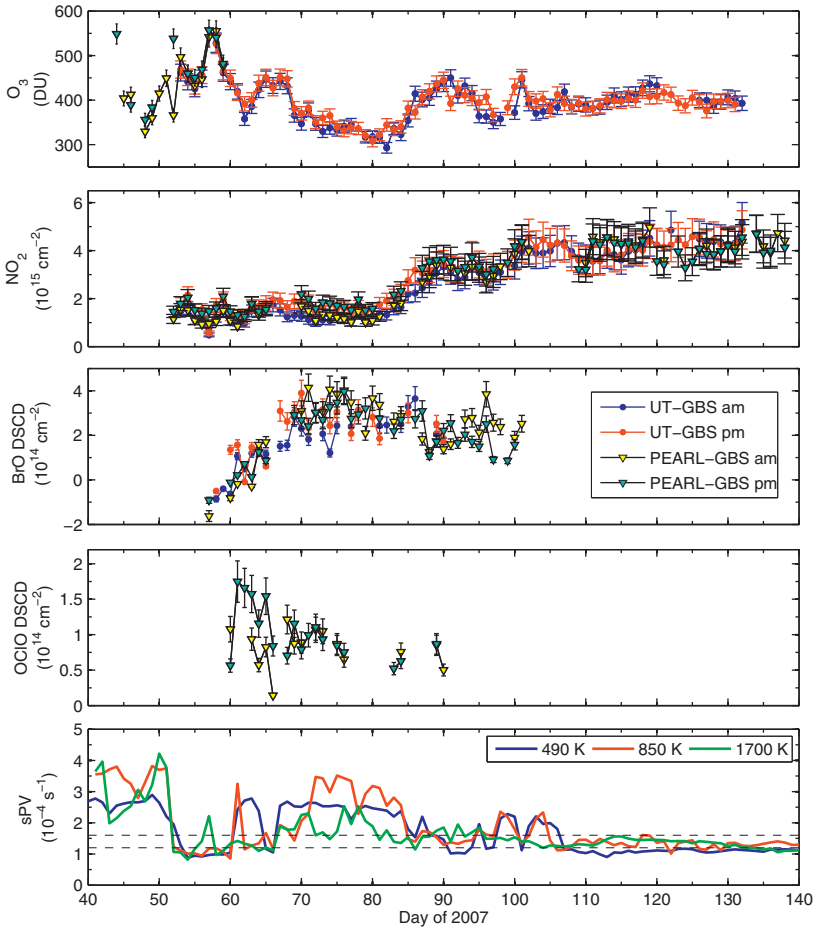

Fig. 8. (a) Ozone and (b) NO_2 VCDs from the UT-GBS and PEARL-GBS for polar sunrise 2007. (c) BrO and (d) OClO DSCDs at 90° and (e) sPV on the 490, 850, and 1700 K potential temperature levels (corresponding to altitudes of 18, 30, and 50 km). The dotted horizontal lines indicate 1.2 and 1.6×10^{-4} s^{-1}, approximately demarking the edges of the polar vortex region.

[42,6,36,43]. The UT-GBS has participated in all six campaigns, while the PEARL-GBS has participated in the 2007–2009 campaigns. The 2007 Canadian Arctic ACE Validation Campaign, discussed herein, was held between February 19 and April 3, 2007.

Ozone and NO_2 VCDs and BrO and OClO DSCDs from the UT-GBS and PEARL-GBS from the campaign are shown in Fig. 8. sPV is also shown on three potential temperature levels: 490 K (∽50 hPa, ∽18 km, lower stratosphere), 850 K (∽10 hPa, ∽30 km, middle stratosphere), and 1700 K (∽1.5 hPa, ∽50 km, upper stratosphere).

In the lower stratosphere, where the peak in ozone number density is found (∽15–20 km), the vortex is over Eureka at the start of the campaign, moves away between days 54 and 60 (February 23 to March 1), is back over Eureka again between day 61 and 64 (March 2–5), and moves away between days 65 and 66 (March 6 and 7). The vortex moves back over Eureka on day 67 (March 8), and stays there until day 90 (March 31). The vortex then moves back and forth over Eureka in April, with Eureka inside the vortex on day 95 (April 5), between days 98 and 100 (April 8–10), and again between day 103 (April 13) and day 106 (April 16). Ozone VCDs are higher when Eureka is outside and on the edge of the vortex. During the three-week period when the vortex remains over Eureka, ozone VCDs are seen to decrease. Once the vortex breaks apart in late March, ozone concentrations are fairly constant through the rest of April and May.

The behaviour of NO_2 during the campaign is dominated by the photolysis of N_2O_5. Morning and afternoon columns begin to agree towards the end of the campaign, as the Sun is continuously above the horizon after April 14 (day 105). The maximum in the NO_2 number density profile is between 25 and 35 km, with significant contributions in the lower stratosphere as well. In the middle stratosphere, the vortex is over Eureka until day 51 (February 20), then moves away until day 61 (March 2), when the vortex moves back over Eureka. The vortex then stays over Eureka until it breaks apart in April. NO_2 is generally increasing during the campaign, as the amount of available sunlight increases. NO_2 VCDs are low at the beginning of the campaign and increase on day 63 when the vortex moves over Eureka. Between days 70 and 80, the sPV values at 850 K become much larger, indicating the centre of the vortex has moved closer to Eureka. When Eureka is

Table 4
OClO DSCDs measured by ground-based zenith-sky spectrometers during Arctic springtime.

Location	OClO DSCD range (10^{14} molecules/cm^2)	Reference
Søndre Strømfjord, Greenland (67°N)	0.5–2.5	Grund et al. [45]
Andøya, Norway (69°N)	0.4–1.3	Tørnkvist et al. [9]
Ny-Ålesund, Norway (79°N)	0.5–1.5	[46]
Ny-Ålesund, Norway (79°N)	0.5–2.0	[9]
Eureka, Canada (80°N)	0.3–4.0	[4]
Eureka, Canada (80°N)	0.1–2.0	This work

deep inside the vortex between days 70 and 80, NO_2 VCDs begin to decrease. Ozone and NO_2 generally follow the same trends throughout the campaign.

The peak in BrO number density is between 10 and 20 km, in the lower stratosphere. BrO DSCDs at 90° are generally increasing at the beginning of the campaign until the vortex moves back over Eureka on day 67 (March 8), when they begin to decrease slightly. They increase when Eureka is outside the vortex at the end of March, and then decrease through April. Once the Sun no longer sets, in mid-April, the DSCD at 90° can no longer be calculated. The BrO columns peak in the middle of the campaign and decrease until the end of the observation period. Similar behaviour was observed by Tørnkvist et al. [9]. Ozone and BrO are generally positively correlated throughout the campaign. NO_2 and BrO are not clearly related until the end of the campaign, after day 90, when NO_2 columns increase while BrO columns decrease, as discussed in the previous section.

The OClO DSCDs in Fig. 8(d) are at 90°, analysed with a daily reference spectrum at 80°, or, before the Sun rises to 80°, the highest SZA possible. The OClO DSCDs increase sharply when the vortex moves over Eureka on day 61, indicating chlorine activation inside the vortex, and steadily decrease during the three-week period when Eureka is inside the vortex in March. The decrease is an indication that active chlorine is being converted to inactive forms. Temperatures in the lower vortex, from GEOS-5 reanalysis (not shown), are constantly above the temperatures required for polar stratospheric cloud formation, indicating that chlorine activation occurred earlier in the winter. There is no strong relationship between OClO and the other species. When the vortex is over Eureka, ozone concentrations decrease from roughly 450 to 300 DU. During this period, the columns of all four species are decreasing. BrO DCDs remain relatively constant during this period. Therefore BrO/ClO-driven catalytic destruction of ozone may have occurred above Eureka.

Table 4 shows OClO DSCDs observed by ground-based zenith-sky viewing grating spectrometers operated in the Arctic during springtime; Farahani [4] used the UT-GBS. Generally a reference spectrum at 80° was used, with the exception of Farahani [4], who used 76°. The range of DSCDs observed during the Eureka 2007 campaign with the PEARL-GBS is consistent with the range of the other observations.

5. Comparisons with other instruments

During the 2007 Canadian Arctic ACE Validation Campaign, the PEARL-GBS and UT-GBS were both operated with the 600 gr/mm grating for approximately one week: from February 24 to 28 (days 53–59). A SAOZ (Sytème d'Analyse par Observations Zénitales) also took part in the campaign and was also installed in a hatch at PEARL. SAOZ is a zenith-sky UV–visible spectrometer that was constructed in the late 1980s and is now deployed in a global network for measurements of stratospheric concentrations of ozone and NO_2 [44]. SAOZ has a similar wavelength range (270–620 nm) and resolution (1.0 nm) to the PEARL-GBS.

The DSCDs and VCDs from the three instruments can be directly compared for this week. The UT-GBS has been compared to the SAOZ previously: during the MANTRA 2004 campaign [3], and during the Eureka campaigns from 2004 to 2006 [6].

5.1. NDACC comparisons

The UV–visible Working Group of NDACC, following three intercomparison campaigns in Lauder, New Zealand [47], the Observatoire de Haute Provence, France [48], and Andøya, Norway [19], has established two sets of protocols for the comparison of ozone and NO_2 DSCDs and VCDs. Type 1 instruments are certified for global studies and trend measurements, while Type 2 instruments are certified for process studies and trend measurements.

For Type 1 comparisons, the DSCDs from two instruments are transformed onto a common SZA grid, using only SZAs between 70° and 91°. A linear regression is performed. The slope of the fit represents how well the two data sets agree: a non-unity slope indicates the DSCDs do not vary with SZA in the same way. A non-zero intercept represents a systematic offset between the two data sets. Residuals are also calculated: those that increase or decrease with SZA indicate non-linear error in at least one of the data sets. In this work, the regression is performed using a least-squares estimation method, and errors in the fit parameters are calculated [49]. Target values are set by NDACC for the slope, intercept, and RMS of the

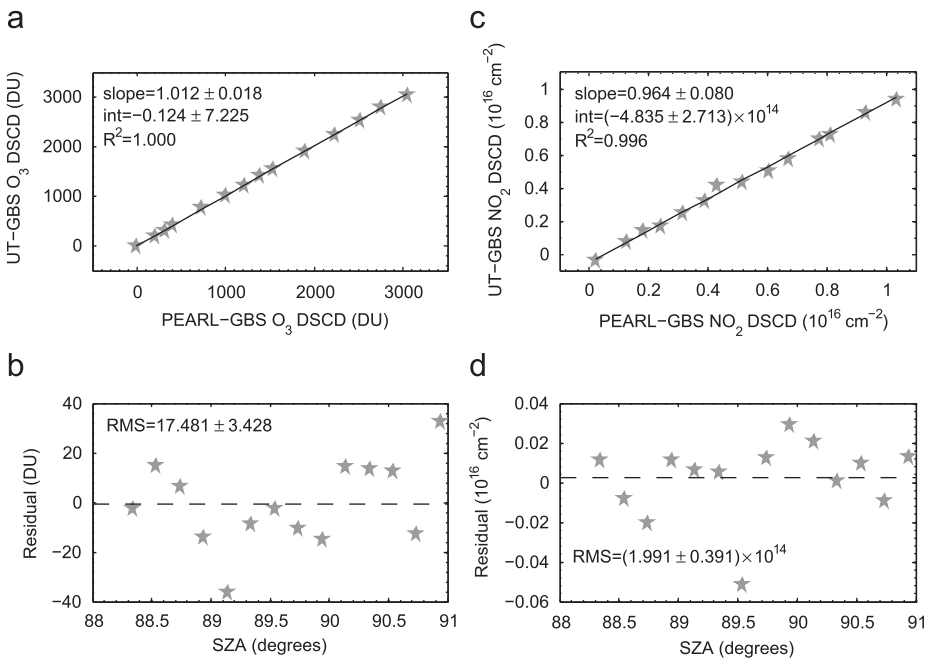

Fig. 9. (a) Type 1 regression analysis for ozone between UT-GBS and PEARL-GBS for sunset, February 27. The solid line indicates the regression fit. (b) Residuals of the fit in (a). The dotted line indicates the average of the residuals. (c) Same as (a), but for NO_2. (d) Same as (b), but for NO_2.

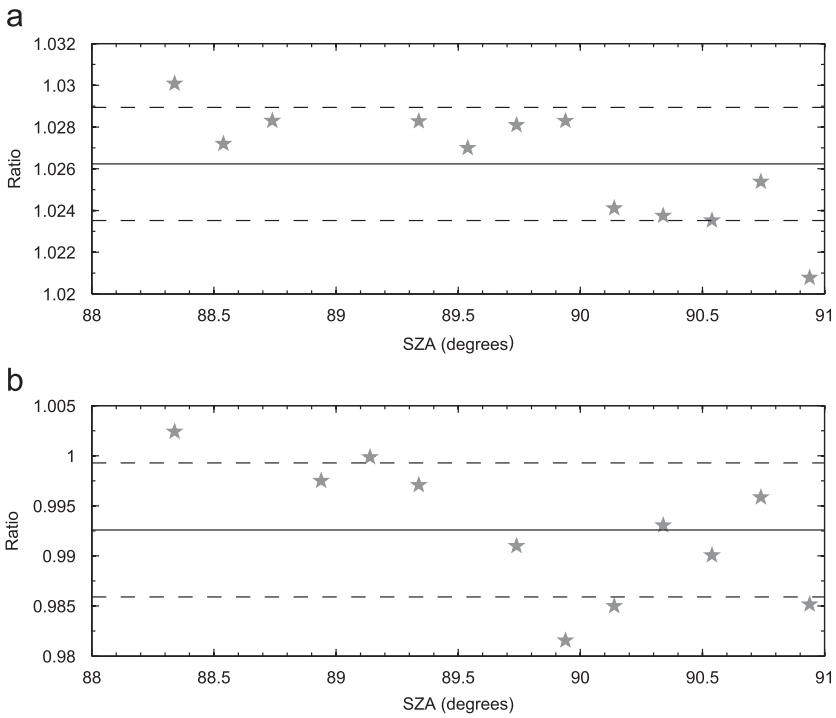

Fig. 10. (a) Type 2 comparisons for ozone between UT-GBS and PEARL-GBS for the afternoon of February 27. The solid line indicates the mean of the ratio between the two instruments, while the dashed lines show the extent of the standard deviation. (b) Same as (a), but for NO_2.

residual for both species. For ozone, the slope should be between 0.97 and 1.03, the intercept should be less than 56 DU, and the RMS of the residual should be less than 37 DU. For NO_2, the slope should be between 0.95 and 1.05, the intercept should be less than 1.50×10^{15} molecules/cm^2, and the RMS of the residual should be less than 1.00×10^{15} molecules/cm^2. An example of this comparison is shown in Fig. 9 for the afternoon of February 27 for the UT-GBS and PEARL-GBS.

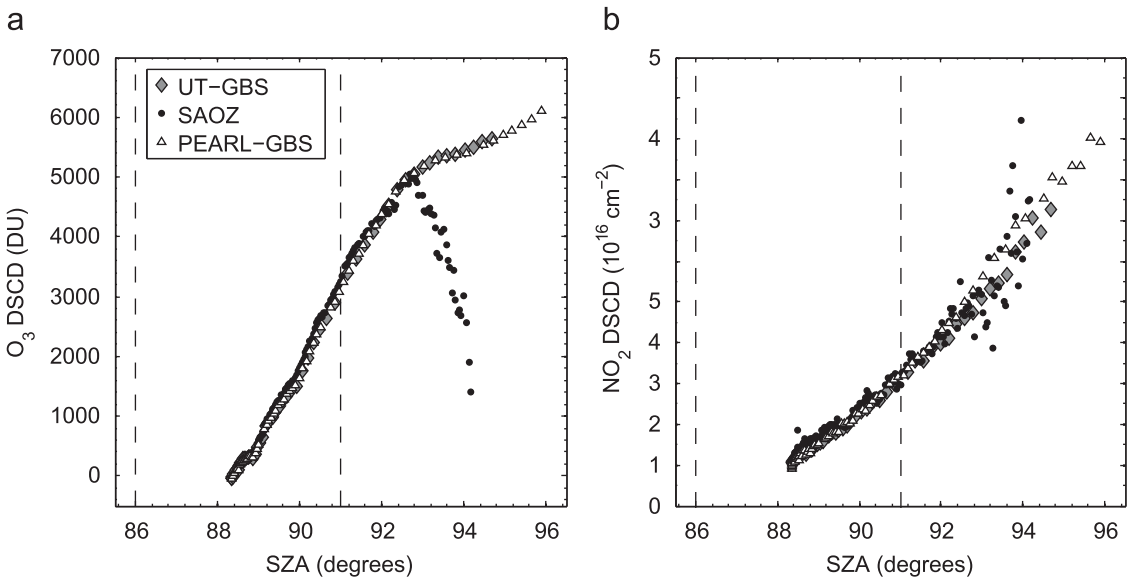

Fig. 11. (a) Ozone DSCDs for the afternoon of February 28, 2007 for the UT-GBS, SAOZ, and PEARL-GBS. (b) Same as (a) but for NO_2. The dashed vertical lines indicate the region of DSCDs used for the calculation of VCDs. For the Type 1 comparisons, DSCDs up to 91° are used. For the Type 2 comparisons DSCDs between 85° and 91° are used, if available.

For Type 2 comparisons, the VCDs from two instruments over the course of a twilight are transformed onto a common SZA grid ranging from 85° to 91° and the ratio of the data from the two instruments is taken. For ozone, the campaign mean of the daily ratios should be in the range from 0.95 to 1.05, with a standard deviation of the mean less than 0.03. For NO_2, the campaign mean of the daily ratios should be between 0.90 and 1.10, with a standard deviation less than 0.05. An example of this comparison is shown in Fig. 10 for the afternoon of February 27 for the UT-GBS and PEARL-GBS.

The PEARL-GBS, UT-GBS, and SAOZ are all zenith-sky-viewing UV–visible spectrometers. All the data from these three instruments have been analysed using WinDOAS with the same wavelength regions and absorption cross-sections. As a result, the ozone and NO_2 DSCDs and VCDs can be compared following the NDACC standards.

5.1.1. Type 1 comparisons

Fig. 11(a) shows the ozone DSCDs for the PEARL-GBS, UT-GBS, and SAOZ for the afternoon of February 28, 2007. Up to roughly 92°, the agreement between the three instruments is good. Beyond this point, the GBS DSCDs continue to agree, while the SAOZ DSCDs diverge to lower DSCDs. This is due to the consistently high temperatures (25–30 °C) inside the viewing hatch of the SAOZ instrument, causing the thermal noise of the spectra to be larger than ideal. As the Sun sets, the constant dark signal (which includes thermal noise) makes up a larger percentage of the total signal, making the data beyond a SZA of 92° unreliable.

Fig. 11(b) shows the NO_2 DSCDs for the PEARL-GBS, UT-GBS, and SAOZ for the same day as the ozone DSCDs. Again the agreement is good up to 92°, when the SAOZ DSCDs become scattered, likely a result of the larger dark signal contribution discussed above. The PEARL-GBS and UT-GBS also begin to diverge at this point, however, this feature is not common to all comparison days.

Fig. 12 shows the results of the Type 1 ozone and NO_2 comparisons for the week when the GBSs were both operating with the 600 gr/mm grating (days 53–59, February 22–28). In all figures, the average parameter is given, with the standard error of the mean ($\sigma/\sqrt{N}$, where σ is the standard deviation, and N is the number of days of comparison) represented as the error bars. The number of twilight periods used in the comparison is given in the figure. NDACC standards are indicated by the dashed lines.

For both species, the PEARL-GBS and UT-GBS mean results meet all three NDACC standards with small standard error, indicating consistency in the comparisons. For ozone, of the individual PEARL-GBS and UT-GBS twilight comparisons (not shown), all 12 comparisons meet the intercept and residual standards, while four of the 12 slopes are outside the NDACC range, though these four agree within the calculated error in the slopes. For NO_2, all but one of the seven individual comparisons meet the slope standards, and all individual comparisons meet the intercept and residual standards.

For ozone, the PEARL-GBS and SAOZ mean results meet all standards with the exception of the afternoon slope, which agrees within the standard error. All 12 individual twilight comparisons (not shown) meet the intercept and residual standards, while six of the 12 slope comparisons are outside the NDACC range. Five of these are in the afternoon. For the NO_2 mean results, the intercept and residual standards are met, while the slopes are outside the desired range. Only one NO_2 individual comparison meets the slope standards, while the intercept and residual standards are consistently met.

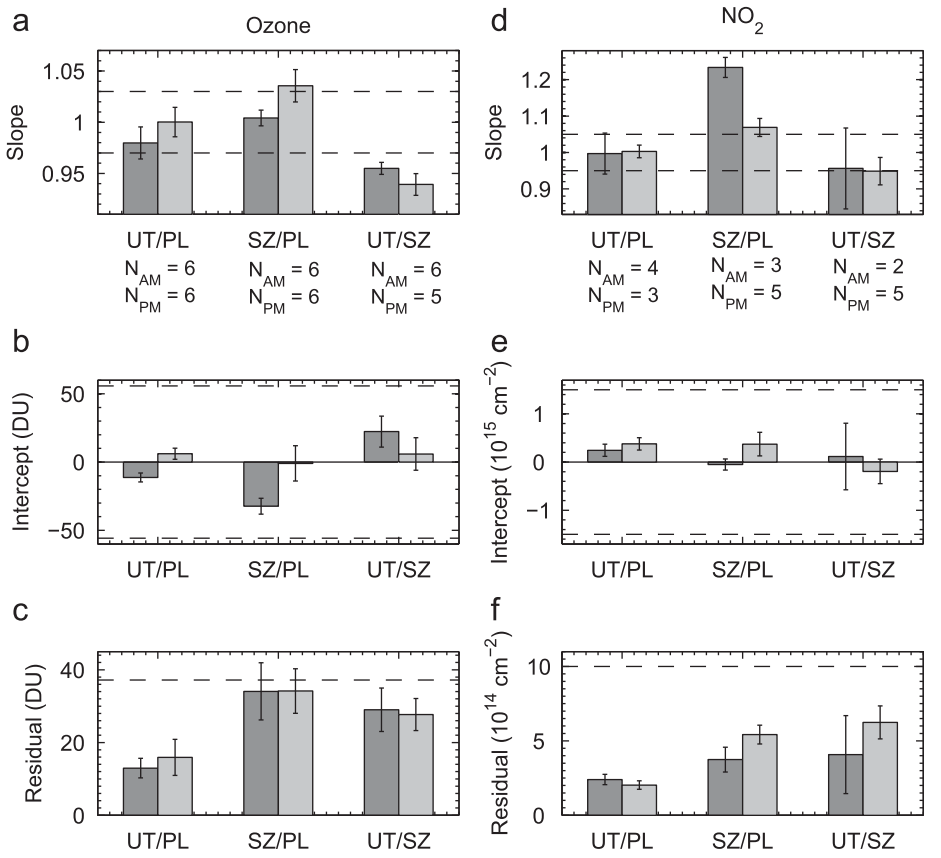

Fig. 12. Type 1 results for the PEARL-GBS, UT-GBS, and SAOZ. (a) Ozone slope results, (b) intercept results, and (c) residual results. (d–f) Same as (a–c), but for NO_2. In all figures, dark grey represents the morning comparisons, while light grey represents the afternoon. Error bars indicate the standard error. Dashed lines indicate the NDACC standards. PL is the PEARL-GBS, UT is the UT-GBS, and SZ is SAOZ. N_{AM} and N_{PM} are the number of morning and evening twilight periods used in the comparisons.

For ozone, the UT-GBS and SAOZ mean results meet the intercept and residual standards, but not the slope standards. This is similar to the agreement seen between these two instruments in previous campaigns at Eureka [6] and mid-latitudes [3]. Eleven of the 12 individual twilight comparisons (not shown) do not meet the standards. For the NO_2 mean results, all three standards are met, again similar to the agreement seen in previous campaigns. For the individual comparisons, all seven meet the intercept and residual standards, while five comparisons meet the slope standards.

It should be noted that these comparisons were performed shortly after polar sunrise, when the Arctic NO_2 column is very small. In addition, there were not many days of possible comparisons. There are fewer NO_2 comparisons than ozone comparisons because of the low amounts of NO_2 and the limited SZA range. SAOZ continued to make ozone and NO_2 measurements until the end of March, while the UT-GBS continued until mid-May. Comparing the data from this extended period (37 days of comparison, February 22 to March 31, days 53–90) does not significantly change the results: the ozone slopes remain smaller than the NDACC standards, while the NO_2 slopes and the intercepts and residuals for both species continue to meet the standards.

5.1.2. Type 2 comparisons

Fig. 13 shows the averaged Type 2 results for ozone and NO_2 for the PEARL-GBS, UT-GBS, and SAOZ. The numbers of twilight periods in the averages are the same as the Type 1 comparisons given in Fig. 12.

As for the Type 1 comparisons, the PEARL-GBS and UT-GBS mean results meet the NDACC standards for the Type 2 comparisons for both species. All of the individual comparisons meet both standards as well.

The PEARL-GBS and SAOZ mean results also meet the Type 2 standards for both species. For ozone, all but one of the 12 individual twilight comparisons meets the ratio standard. For NO_2, three of the eight individual comparisons do not meet the ratio standard.

For ozone, the UT-GBS and SAOZ mean results meet the standard deviation standard, but not the ratio standard, although the values do agree within the standard error. Six of the 12 individual comparisons fall outside of the desired range. For NO_2, the average ratios meet the standards, while the standard deviations are larger than required. Six of the seven individual comparisons do not meet the ratio standard, as evidenced by the large standard error: that the average

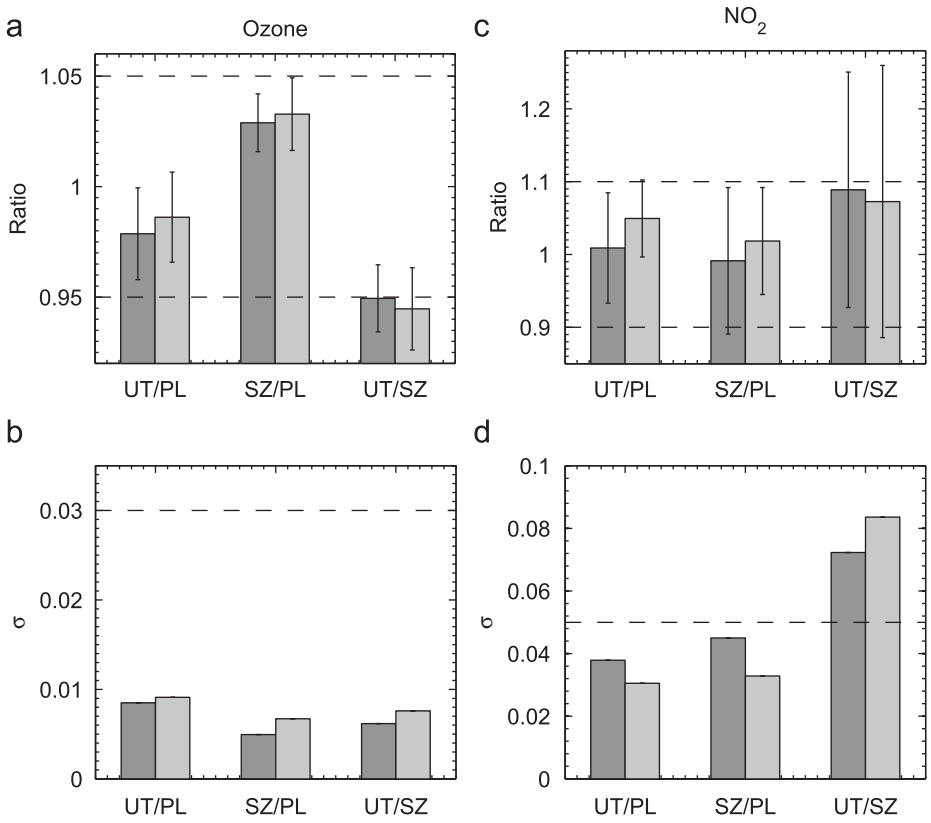

Fig. 13. Type 2 (a) ratio and (b) standard deviation results for ozone. (c–d) Same as (a–b) but for NO_2. The dashed lines indicate the NDAAC standards. Shading and error bars represent the same as in Fig. 12.

does is coincidence. If the entire campaign is considered, amounting to 37 days of comparison (February 22 to March 31), the standards are met for both species' mean results, and the individual twilight comparisons tend to meet the ratio standards. This agreement of ratios over the campaign is similar to the agreement seen in previous campaigns for these two instruments. Previously, the standard deviations have been larger than the NDACC standard.

5.2. Vertical column densities

5.2.1. Ozone

Fig. 14(a) and (b) shows the morning and afternoon ozone VCDs, respectively, from the PEARL-GBS, UT-GBS, SAOZ, and ozonesondes during the 2007 campaign. The sondes are primarily launched at 18:15 LT, although a few are shifted to match the time of the ACE satellite overpasses.

In the following, the average percentage difference is calculated using

$$PD = 100 \times \frac{1}{n}\sum_{i=1}^{n}\frac{data_{1,i} - data_{2,i}}{average_i} \tag{2}$$

PD is the percentage difference, $data_1$ and $data_2$ are the two data sets being compared, *average* is the average of the two data sets, n is the number of days of comparison, and i is the day index.

The average difference between the PEARL-GBS and the UT-GBS during the week-long period at the end of February when both instruments were simultaneously measuring ozone is 15.3 DU (3.2%) (PEARL-GBS minus UT-GBS). The average difference between the PEARL-GBS and SAOZ is −12.4 DU (−2.4%). The average difference between the UT-GBS and SAOZ for the same time period is −11.4 DU (−2.3%); for the entire campaign the average difference between these two instruments is −5.1 DU (−1.2%). Generally, as is seen in Figs. 14(a) and (b), the instruments agree within their error bars, given in Table 3. The same error bar values are used for the UT-GBS and SAOZ. There is no systematic difference between any of the ground-based instruments.

During the last week of February, the integrated columns from the ozonesondes agree with the PEARL-GBS, UT-GBS, and SAOZ to an average of −4.1 DU (−1.2%), 25.6 DU (5.7%), and 6.3 DU (1.3%), respectively (sonde minus ground-based instrument). Sondes are launched weekly at the Eureka Weather Station, and so comparisons are possible throughout the

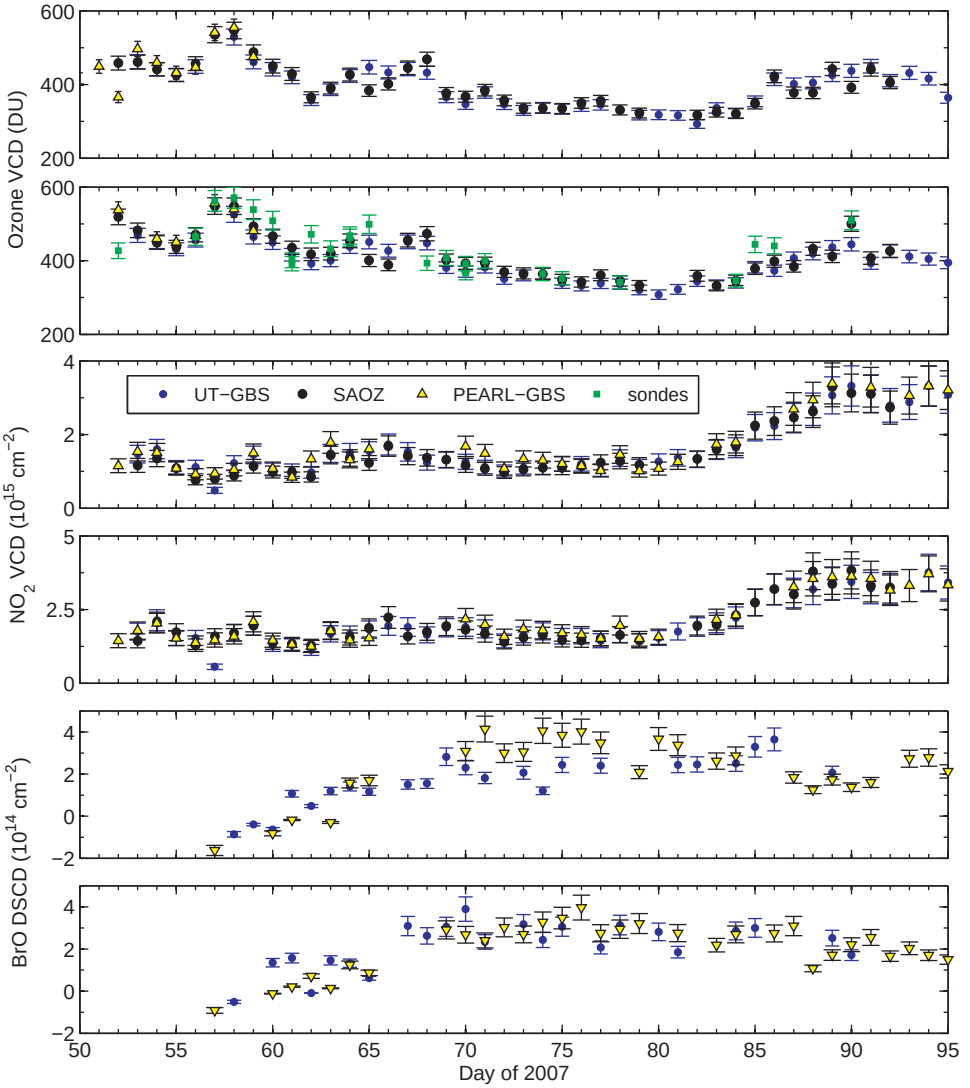

Fig. 14. Ozone (a) AM and (b) PM and NO_2 (c) AM and (d) PM VCDs and BrO (e) AM and (f) PM DSCDs from the PEARL-GBS, UT-GBS, SAOZ, and ozonesondes during the 2007 Canadian Arctic ACE Validation Campaign.

entire time the PEARL-GBS is measuring ozone. The average difference between the sonde columns and the PEARL-GBS from August 2006 to October 2007 is 5.6 DU (2.2%). This represents 22 comparisons, with 1–6 days to compare each month. Generally the columns agree within error bars, with the exception of the end of August and beginning of September 2007 (see Fig. 5).

5.2.2. NO_2

Fig. 14(c) and (d) shows the morning and afternoon NO_2 VCDs from the PEARL-GBS, UT-GBS, and SAOZ during the 2007 campaign. As for ozone, the instruments generally agree within their error bars, with no systematic differences. The average difference between the PEARL-GBS and UT-GBS during the campaign is 0.97×10^{14} molecules/cm^2 (5.9%) (PEARL-GBS minus UT-GBS). The average difference between the PEARL-GBS and SAOZ is 1.22×10^{14} molecules/cm^2 (8.1%). The average difference between the UT-GBS and SAOZ is 0.09×10^{14} molecules/cm^2 (1.0%). The PEARL-GBS was measuring in a different wavelength region in March and April, and the NO_2 DSCDs could not be determined in the same wavelength region as the UT-GBS and SAOZ. However, the agreement between the instruments is similar when examining each measuring period separately. For the week when all three instruments were measuring the same wavelength region, the average differences between the PEARL-GBS and the UT-GBS and SAOZ are 0.55×10^{14} molecules/cm^2 (7.4%) and 1.05×10^{14} molecules/cm^2 (9.0%), respectively. This week occurred at the end of February, when NO_2 levels are low. Although the percentage differences are larger than the comparisons using the whole campaign, the differences in VCDs are similar.

Table 5
Average percent differences between the three ground-based instruments for ozone and NO_2 VCDs and BrO DSCDs.

Species	PL minus UT (%)	PL minus SZ (%)	UT minus SZ (%)	Combined error(%)
Ozone	3.2	−2.4	−2.3	5.8
NO_2	5.9	8.1	1.0	23.2
BrO	13.1	–	–	20.9

Also given is the combined error, calculated from the individual error bars combined in quadrature. PL indicates the PEARL-GBS, UT the UT-GBS, and SZ the SAOZ.

5.2.3. BrO DSCDs

Fig. 14(e) and (f) shows the morning and afternoon BrO DSCDs from the PEARL-GBS and UT-GBS during the 2007 campaign. Once again, the two instruments typically agree within error bars, with no systematic differences. The average difference between the two instruments is 1.68×10^{13} molecules/cm^2 (13.1%).

6. Summary and future work

The PEARL-GBS was successfully installed at PEARL in August 2006 as part of the refurbishment of the facility undertaken by CANDAC. It has since been making continuous measurements, except during polar night. VCDs of ozone, NO_2, and BrO have been retrieved from the UV–visible zenith-sky spectra. DSCDs of OClO have also been retrieved.

The ozone and NO_2 DSCDs from the instrument have been compared to those from the UT-GBS and SAOZ following the protocols of the UV–visible Working Group of the NDACC. The PEARL-GBS and UT-GBS have been found to meet the required accuracies for both species. The comparisons between the other two pairs of instruments are found to partially meet the required standards.

The ozone and NO_2 VCDs and BrO DSCDs from the three ground-based instruments have also been compared and are found to agree within the combined error bars of the three species. The average percent differences, along with the combined error bars, are given in Table 5. The ozone VCDs are further compared to the integrated total columns from ozonesondes launched at Eureka, and agree within combined error bars (6.5%).

Both the PEARL-GBS and UT-GBS continue to operate at PEARL. In February 2008, a suntracker was installed above the PEARL-GBS. During the 2008 and 2009 Canadian Arctic ACE Validation Campaigns, the PEARL-GBS made observations of the direct Sun on clear days, while the UT-GBS continued zenith-sky measurements. Using an optimal estimation method, the BrO columns from the two instruments can be separated into tropospheric and stratospheric components [50–52]. The suntracker can also be used to perform Multi-AXis DOAS (MAX-DOAS) measurements [53,54], which are more complicated to interpret than the direct Sun measurements, but can also yield low-resolution vertical profiles of BrO. Either of these configurations should allow for the observation of "bromine explosions", which occur in the Arctic troposphere in the late spring [55], and possibly tropospheric IO [56]. The suntracker can also be configured to track the Moon, which could extend measurements through the polar night. Analysis of the spectra recorded during these campaigns is underway.

Acknowledgements

CANDAC and PEARL are funded by the Atlantic Innovation Fund/Nova Scotia Research Innovation Trust, Canadian Foundation for Climate and Atmospheric Science, Canadian Foundation for Innovation, the Canadian Space Agency (CSA), Environment Canada (EC), Government of Canada International Polar Year funding, the Natural Sciences and Engineering Research Council of Canada (NSERC), Ontario Innovation Trust, Polar Continental Shelf Program and the Ontario Research Fund. Thanks to Pierre Fogal, the PEARL Operations Manager and Keith MacQuarrie, a CANDAC operator, for help installing the PEARL-GBS. Thanks also to Pierre, and to Ashley Harrett, Alexei Khmel, Paul Loewen, Oleg Mikhailov, and Matt Okraszewski, the CANDAC operators, for maintaining both instruments at PEARL.

The Canadian Arctic ACE Validation Campaign project has been supported by the CSA, EC, NSERC, the Northern Scientific Training Program and the Centre for Global Change Science at the University of Toronto. The campaigns are co-led by Kaley A. Walker of the University of Toronto. Logistical and on-site technical support for the 2007 campaign was provided by CANDAC. The SAOZ participation in the campaign was supported by the Centre National D'Études Spatiales.

WinDOAS was provided by C. Fayt and M. Van Roozendael of the Belgian Institute for Space Aeronomy (IASB-BIRA). Chris McLinden of EC provided the radiative transfer model.

We acknowledge William Daffer of JPL for his assistance in performing the sPV calculations. Work at the Jet Propulsion Laboratory, California Institute of Technology was done under contract with the National Aeronautics and Space Administration.

Thanks to the staff of the Eureka Weather Station for the ozonesonde launches and their hospitality during the campaigns.

We also thank the two anonymous reviewers whose comments helped to improve this manuscript.

References

[1] Bassford MR, Strong K, McLinden CA. Zenith-sky observations of stratospheric gases: the sensitivity of air mass factors to geophysical parameters and the influence of tropospheric clouds. JQSRT 2001;68:657–77.
[2] Bassford MR, Strong K, McLinden CA, McElroy CT. Ground-based measurements of ozone and NO_2 during MANTRA 1998 using a zenith-sky spectrometer. Atmos Ocean 2005;43:325–38.
[3] Fraser A, Bernath PF, Blatherwick RD, Drummond JR, Fogal PF, Fu D, et al. Intercomparison of ground-based ozone and NO_2 measurements during the MANTRA 2004 campaign. Atmos Chem Phys 2007;7:5489–99.
[4] Farahani E. Stratospheric composition measurements in the Arctic and at mid-latitudes and comparison with chemical fields from atmospheric models. PhD thesis, University of Toronto; 2006.
[5] Farahani E, Strong K, Mittermeier RL, Fast H Van Roozendael M, Fayt C. Springtime Arctic ground-based spectroscopy of O_3 and related trace gases at Eureka, Canada: part I—evaluation of the analysis method and comparison with infrared measurements. Atmos Meas Tech Discuss 2009;2:343–77.
[6] Fraser A, Goutail F, Strong K, Bernath PF, Boone C, Daffer WH, et al. Intercomparison of UV–visible measurements of ozone and NO_2 during the Canadian Arctic ACE Validation Campaigns: 2004–2006. Atmos Chem Phys 2008;8:1763–88.
[7] Farman JC, Gardiner BG, Shanklin JD. Large loses of total ozone in Antarctica reveal seasonal ClO_x/NO_x interaction. Nature 1985;315:207–10.
[8] Rowland FS. Stratospheric ozone depletion. Philos Trans R Soc B 2006;361:769–90.
[9] Tørnkvist KK, Arlander DW, Sinnhuber BM. Ground-based UV measurements of BrO and OClO over Ny-Ålesund during winter 1996 and 1997 and Andøya during winter 1998/99. J Atmos Chem 2002;43:75–106.
[10] Solomon S, Schmeltekopf AL, Sanders RW. On the interpretation of zenith sky absorption measurements. J Geophys Res 1987;92:8311–9.
[11] Platt U. Differential optical absorption spectroscopy. In: Sigrist M, editor. Air monitoring by spectroscopic techniques. Hoboken, NJ: Wiley; 1994. p. 27–84.
[12] Burrows JP, Richter A, Dehn A, Deters B, Himmelmann S, Voight S, et al. Atmospheric remote-sensing reference data from GOME. 2. Temperature dependent absorption cross-sections of O_3 in the 231–794 nm range. JQSRT 1999;61:509–17.
[13] Vandaele AC, Hermans C, Simon PC, Carleer M, Colin R, Fally S, et al. Measurements of the NO_2 absorption cross-section from 42 000 cm^{-1} to 10 000 cm^{-1} (238–1000 nm) at 220 K and 294 K. JQSRT 1998;59:171–84.
[14] Rothman LS, Barbe A, Benner DC, Brown LR, Camy-Peyret C, et al. The HITRAN molecular spectroscopic database: edition of 2000 including updates through 2001. JQSRT 2003;82:5–44.
[15] Greenblatt GF, Orlando JJ, Burkholder JB, Ravishankara AR. Absorption measurements of oxygen between 330 and 1140 nm. J Geophys Res 1990;95:18577–82.
[16] Wilmouth DM, Hanisco TF, Donahue NM, Anderson JG. Fourier transform ultraviolet spectroscopy of the $A\,^2\pi_{3/2} \leftarrow X^2\pi_{3/2}$ transition of BrO. J Phys Chem A 1999;103:8935–45.
[17] Wahner A, Tyndall GS, Ravishankara AR. Absorption cross sections for symmetric chlorine dioxide as a function of temperature in the wavelength range 240–480 nm. J Phys Chem 1987;91:2734–8.
[18] Chance KV, Spurr RJD. Ring effect studies: Rayleigh scattering, including molecular parameters for rotational Raman scattering, and the Fraunhofer spectrum. Appl Opt 1997;36:5224–30.
[19] Vandaele AC, Fayt C, Hendrick F, Hermans C, Humbled F, et al. An intercomparison campaign of ground-based UV–visible measurements of NO_2, BrO, and OClO slant columns: methods of analysis and results for NO_2. J Geophys Res 2005;110, doi:10.1029/2004JD005423.
[20] Aliwell SR, Van Roozendael M, Johnston PV, Richter A, Wagner T, et al. Analysis for BrO in zenith-sky spectra: an intercomparison exercise for analysis improvement. J Geophys Res 2002;107, doi:10.1029/2001JD000329.
[21] Fayt C, Van Roozendael M. WinDOAS 2.1—software user manual. Belgium: Uccle; 2001.
[22] McLinden CA, McConnell JC, Griffioen E, McElroy CT. A vector radiative-transfer model for the Odin/OSIRIS project. Can J Phys 2002;80:375–93.
[23] Prather MJ. Catastrophic loss of stratospheric ozone in dense volcanic clouds. J Geophys Res 1997;97:10187–91.
[24] McLinden CA, Olsen SC, Hannegan B, Wild O, Prather MJ, Sundet J. Stratospheric ozone in 3-D models: a simple chemistry and the cross-tropopause flux. J Geophys Res 2000;105:14653–65.
[25] Sarkissian A, Vaughan G, Roscoe HK, Bartlett LM, O'Conner FM, Drew DG, et al. Accuracy of measurements of total ozone by a SAOZ ground-based zenith sky visible spectrometer. J Geophys Res 1997;102:1379–90.
[26] Otten C, Ferleman U, Platt U, Wagner T, Pfeilsticker K. Groundbased DOAS UV/visible measurements at Kiruna (Sweden) during the SESAME winters 1993/94 and 1994/95. J Atmos Chem 1998;30:141–62.
[27] Oetjen H, Bovensmann H, Medeke T, Richter A, Sheode N. Comparison of modelled and measured chlorine dioxide slant columns for the Arctic winter. In: Proceedings of the 3rd workshop in the Atmospheric Chemistry Validation of ENVISAT (ACVE-3), ESRIN, Frascati, Italy, 4–7 December 2006, ESA SP-642, 2007.
[28] Pfeilsticker K, Erle F, Platt U. Observation of the stratospheric NO_2 latitudinal distribution in the northern winter hemisphere. J Atmos Chem 1999;32:101–20.
[29] Harder H, Bösch H, Camy-Peret C, Chipperfield MP, Fitzenberger R, Payan S, et al. Comparison of measured and modeled stratospheric BrO: implications for the total amount of stratospheric bromine. Geophys Res Lett 2000;27:3695–8s.
[30] Fish DJ, Jones RL. Rotational Raman scattering and the Ring effect in zenith-sky spectra. Geophys Res Lett 1995;22:811–4.
[31] Tarasick DW, Fioletov VE, Wardle DI, Kerr JB, Davies J. Changes in the vertical distribution of ozone over Canada from ozonesondes: 1980–2001. J Geophys Res 2005;110, doi:10.1029/2004JD004643.
[32] Stratospheric processes and their role in climate (SPARC): assessment of trends in the vertical distribution of ozone. SPARC Report no. 1. In: Harris N, Hudson R, Phillips C, editors. WMO global ozone research and monitoring project. Report 43. Geneva: World Meteorological Organization; 1998.
[33] Reinecker MM, et al. The GEOS-5 data assimilation system: a documentation of GEOS-5.0. Technical Report 104606 V27, NASA, 2008.
[34] Manney GL, Zurek RW, O'Neill A, Swinbank R. On the motion of air through the stratospheric polar vortex. J Atmos Sci 1994;51:2973–94.
[35] Manney GL, Daffer WH, Zawodny JM, Bernath PF, Hoppel KW, et al. Solar occultation satellite data and derived meteorological products: sampling issues and comparisons with Aura MLS. J Geophys Res 2007;112, doi:10.1029/2007JD008709.
[36] Manney GL, Daffer WH, Strawbridge KB, Walker KA, Boone CD, Bernath PF, et al. The High Arctic in extreme winters: vortex, temperature, and MLS and ACE-FTS trace gas evolution. Atmos Chem Phys 2008;8:505–22.
[37] Hood LL, Soukharev BE, Fromm M, McCormak JP. Origin of extreme ozone minima at middle to high northern latitudes. J Geophys Res 2001;106:20925–40.
[38] Sinnhuber BM, Arlander DW, Bovensmann H, Burrows JP, Chipperfield MP, et al. Comparison of measurements and model calculations of stratospheric bromine monoxide. J Geophys Res 2002;107, doi:10.1029/2002JD000940.
[39] Richter A, Eisinger M, Ladstätter-Weißenmayer A, Burrows JP. DOAS zenith sky observations: 2. Seasonal variations of BrO over Bremen (53°N) 1994–1995. J Atmos Chem 1999;32:83–99.
[40] Danilin MY, McConnell JC. Stratospheric effects of bromine activation on/in sulfate aerosol. J Geophys Res 1995;100:11237–43.
[41] Bernath PF, McElroy CT, Abrams MC, Boone CD, Butler M, et al. Atmospheric chemistry experiment (ACE): mission overview. Geophys Res Lett 2005;32 doi:10.1029/2005GL0022386.
[42] Kerzenmacher TE, Walker KA, Strong K, Berman R, Bernath PF, Boone CD, et al. Measurements of O_3, NO_2 and temperature during the 2004 Canadian Arctic ACE Validation Campaign. Geophys Res Lett 2005;32 doi:10.1029/2005GL023032.

[43] Fu D, Walker KA, Mittermeier RL, Strong K, Sung K, Fast H, et al. Simultaneous atmospheric measurements using two Fourier transform infrared spectrometers at the Polar Environment Atmospheric Research Laboratory during spring 2006, and comparisons with the Atmospheric Chemistry Experiment-Fourier Transform Spectrometer. Atmos Chem Phys Discuss 2008;8:5305–58.
[44] Pommereau JP, Goutail F. O_3 and NO_2 ground-based measurements by visible spectroscopy during Arctic winter and spring 1988. Geophys Res Lett 1988;15:891–4.
[45] Grund A, Klüpfel T, Grendel A, Krug B, Perner D. Ozone depletion potential from stratospheric OClO and BrO observations during Arctic winters 1992–96 and the comparison with observed ozone columns. In: Bojkov RD, Viscounti G, editors. Proceedings of the XVIII quadrennial ozone symposium, vol. 1, L'Aquila, Italy, 12–21 September 1996, 1998. p. 209–12.
[46] Wittrock F, Eisinger M, Ladstätter-Weißenmayer A, Richter A, Burrows JP. Ground-based UV-VIS measurements of O_3, NO_2, OClO, and BrO over Ny-Ålesund (79°N, 12°E). In: Bojkov RD, Viscounti G, editors. Proceedings of the XVIII quadrennial ozone symposium, vol. 1, L'Aquila, Italy, 12–21 September 1996, 1998. p. 623–6.
[47] Hoffman D, Bonasoni P, De Maziere M, Evangelisti F, Giovanellie G, et al. Intercomparison of UV/visible spectrometers for measurements of stratospheric NO_2 for the network for the detection of stratospheric change. J Geophys Res 1995;100:16765–91.
[48] Roscoe HK, Johnston PV, Van Roozendael M, Richter A, Sarkissian A, et al. Slant column measurements of O_3 and NO_2 during the NDSC intercomparison of zenith-sky UV–vis spectrometers in June 1996. J Atmos Chem 1999;32:281–314.
[49] York D, Evensen NM, López Martínez M, De Basabe Delgado J. Unified equations for the slope, intercept, and standard errors of the best straight line. Am J Phys 2004;72:367–75.
[50] Schofield R, Connor BJ, Kreher K, Johnston PV, Rodgers CD. The retrieval of profile and chemical information from ground-based UV–visible spectroscopic measurements. JQSRT 2003;86:115–31.
[51] Schofield R, Kreher K, Connor BJ, Johnston PV, Thomas A, Shooter D, et al. Retrieved tropospheric and stratospheric BrO columns over Lauder, New Zealand. J Geophys Res 2004;109 doi:10.1029/2003JD004463.
[52] Schofield R, Johnston PV, Thomas A, Kreher K, Connor BJ, Wood S, et al. Tropospheric and stratospheric BrO columns over Arrival Heights, Antarctica, 2002. J Geophys Res 2006;111 doi:10.1029/2005JD007022.
[53] Hönninger G, Platt U. Observations of BrO and its vertical distribution during surface ozone depletion at Alert. Atmos Environ 2002;36:2481–9.
[54] Hönninger G, von Friedeberg C, Platt U. Multi axis differential optical absorption spectroscopy (MAX-DOAS). Atmos Chem Phys 2004;4:231–54.
[55] McElroy CT, McLinden CA, McConnell JC. Evidence for bromine monoxide in the free troposphere during the Arctic polar sunrise. Nature 1999;397:338–41.
[56] Schönhardt A, Richter A, Wittrock F, Kirk H, Oetjen H, Roscoe HK, et al. Observations of iodine monoxide columns from satellite. Atmos Chem Phys 2008;8:637–53.